Some properties of speckle from smooth objects

Joseph W. Goodman, FELLOW SPIE
570 University Terrace
Los Altos, California 94022
E-mail: jwgood@me.com

Abstract. We explore certain symmetry properties of the Fourier spectrum of speckle from smooth objects and the effects of these symmetries on image speckle contrast. The cases examined include bright-field imaging, dark-field imaging, and single-sideband imaging. [DOI: 10.1117/1.3454387]

Subject terms: speckle; surface roughness; microscopy.

Paper 100295R received Apr. 5, 2010; revised manuscript received Apr. 26, 2010; accepted for publication May 3, 2010; published online Jun. 23, 2010.

1 Introduction

This paper is concerned with speckle produced by objects that can be described as *smooth*, by which we mean objects that, in transmission or reflection, produce random phase fluctuations that are small compared with 2π rad. For illustration purposes, we assume a transmission geometry, but the same arguments apply, with minor changes, to reflection geometries.

There is a considerable history of studies of measurement of surface roughness using speckle, but most of this work is aimed at surfaces that are not smooth in the sense defined. Exceptions are multiple works by Asakura and his colleagues (see for example Refs. 1 and 2), Pederson,[3] and Goodman.[4] An early review of this subject was published by Welford.[5] In addition, relevant related work has been published in the astronomy literature, particularly on the properties of speckle produced in coronagraph images with imperfectly corrected adaptive optics systems.[6–8]

For future reference, it should be noted that a wavefront that is smooth in the sense defined and has a wavefront roughness that obeys spatially stationary Gaussian statistics consists of two components: a specular component containing a fraction $\exp(-\sigma_\phi^2)$ of the total power, and a diffuse component carrying a fraction $1-\exp(-\sigma_\phi^2)$ of the total power (see Ref. 9, Sec. 8.3.2). Depending on the details of the imaging system, the light intensity in the image plane will consist of either interference of the transmitted specular and diffuse components of the light, or, in the event that the specular component is blocked, simply the intensity associated with the transmitted diffuse component of the light.

The geometry assumed here is shown in Fig. 1. A uniform diffuser is normally illuminated by a unit-amplitude, monochromatic, polarized plane wave, and the transmitted field is then imaged by a $4f$ imaging system. The resolution of the system is determined by the extent of the pupil stop in the focal plane of the first lens, where the incident field is the scaled Fourier transform of the complex amplitude distribution transmitted by the diffuser. Our approach is to find properties of speckle by simulation, and then to explain the origins of these properties by means of continuous (as opposed to discrete) reasoning. The simulations are all one-dimensional, but similar results hold if they are extended to two dimensions.

2 Speckle Symmetry in the Fourier Domain

Distributions of speckle intensity were calculated for various standard deviations of a zero-mean Gaussian random phase function. The simulation involved defining a discrete sequence representing a random phase function $\phi(x)$, substituting it as the argument of $\exp[j\phi(x)]$, calculating the Fourier transform by means of a fast Fourier transformation (FFT), and taking the squared modulus of the result, which represents the focal plane intensity. The length of the random phase sequence for this calculation was 256, and the phase samples in the object plane were uncorrelated. The object intensity distribution was thus assumed uniform.

Note that while aliasing is present in the Fourier plane due to the uncorrelated phase sequence used, we argue that it does not change the *statistics* of the observed focal plane intensity, because aliasing simply adds uncorrelated random walks to the random walk found at each frequency, and sums of uncorrelated random walks on an amplitude basis result in a new random walk with the same length and phase statistics as any of the component walks. The properties of the Fourier speckle of most interest here are also shown to be predicted by continuous reasoning, for which no aliasing exists.

In Fig. 2, a series of one-dimensional Fourier-plane speckle pattern intensities is shown, obtained as described. Progression from (a) through (d) in the figure corresponds to decreasing phase standard deviation, as explained in the caption and labeled on the figure. The zero-frequency component of the spectrum has been shifted to the center of the distribution. Symmetry about the zero-frequency (or specu-

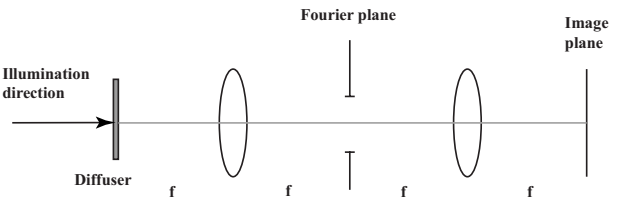

Fig. 1 Imaging geometry.

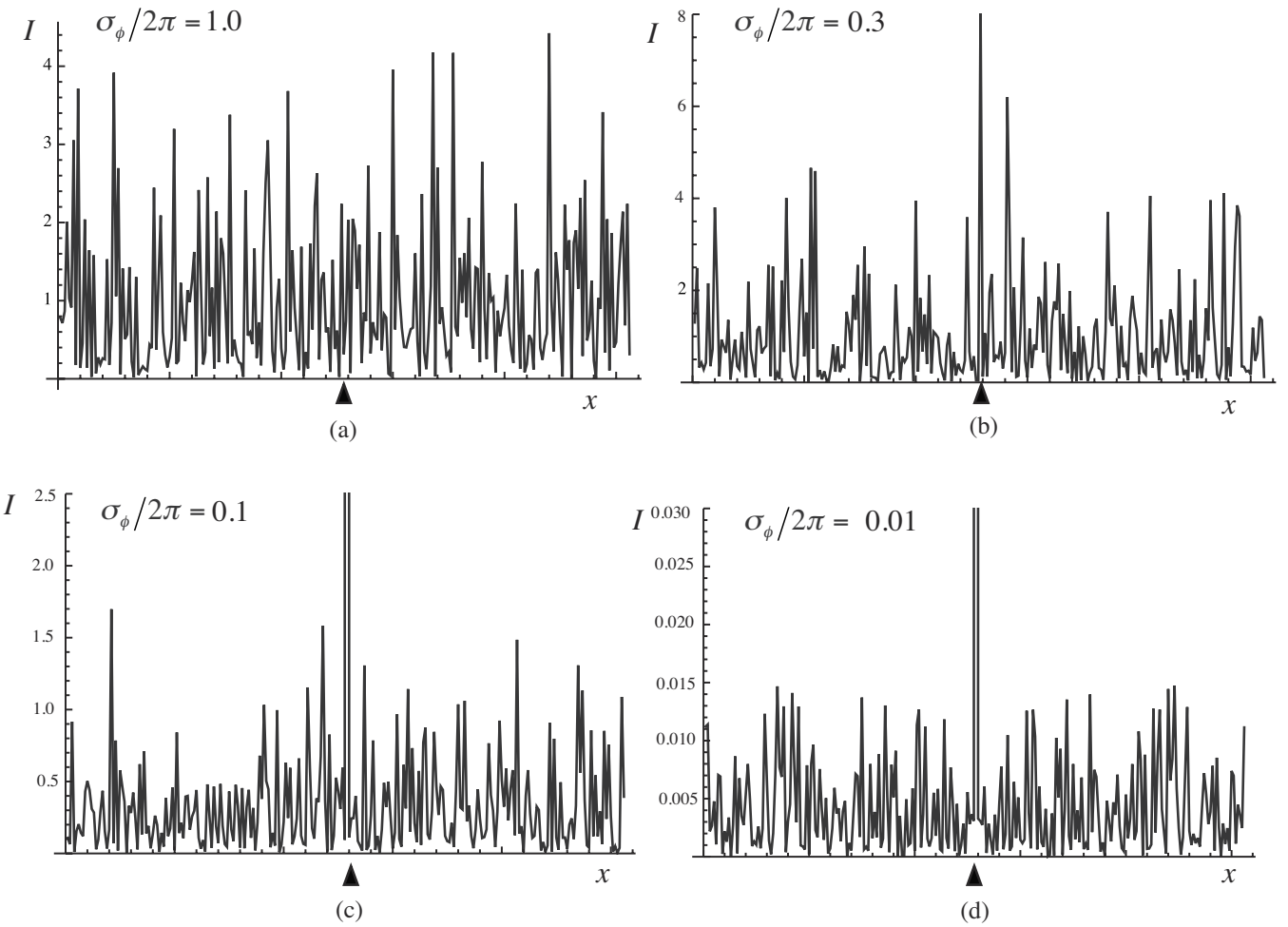

Fig. 2 Speckle pattern intensities obtained for decreasing phase standard deviation: (a) $\sigma_\phi/2\pi=1$, (b) $\sigma_\phi/2\pi=0.3$, (c) $\sigma_\phi/2\pi=0.1$, (d) $\sigma_\phi/2\pi=0.01$. The arrowhead indicates the location of the zero-frequency (specular) component, which in (c) and (d) extends beyond the upper limit of the plot. Note the increasing appearance of symmetry about the specular component as we progress from (a) through (d).

lar) component is seen to grow with decreasing phase standard deviation, resulting in near-perfect symmetry in part (d).

Why do such symmetries appear? The explanation is as follows. For very small σ_ϕ, the complex light amplitude transmitted by the diffuser can be modeled as

$$U_0(x) = \exp[j\phi(x)] \approx 1 + j\phi(x), \tag{1}$$

where $\phi(x)$ is a real-valued Gaussian random phase process. We have ignored the rectangular spatial bound on the object for mathematical simplicity; including the bound does not change our results in any substantive way. In the Fourier domain (which is equivalent to the focal plane if we ignore spatial scaling factors), the equivalent expression is

$$\mathcal{U}_0(\nu) \approx \delta(\nu) + j\Phi(\nu). \tag{2}$$

Since $\phi(x)$ is real-valued, it follows that $\Phi(\nu)$ has a real part that is an even function of ν and an imaginary part that is an odd function of ν. As a consequence, $j\Phi(\nu)$ has an odd real part and an even imaginary part. More importantly, $|j\Phi(\nu)|^2$ is a purely even, real function. Thus we see that, in the limit of very small σ_ϕ, the speckle pattern takes on the form of a narrow and strong specular component at the origin in the spectral domain, and a diffuse random component with an intensity distribution $|\Phi(\nu)|^2$ that is an even function of ν about the location of the specular component.

The symmetry of the focal plane distribution of speckle under small phase-variance conditions has been noticed before in astronomy, in particular for coronagraph imaging in adaptive optics systems that do not completely compensate for atmospheric wavefront deformations. See Refs. 6–8. However, the astronomical systems differ from that studied here in that the random phase deformations occur in what would be the pupil plane of our system, with the image again being observed in what we have labeled the image plane. In the $4f$ system of interest here, the phase structure and the image are in conjugate planes, and we wish to quantify the effects of Fourier-plane symmetry on the speckle obtained in the image plane.

It is possible to quantify the correlation of the Fourier

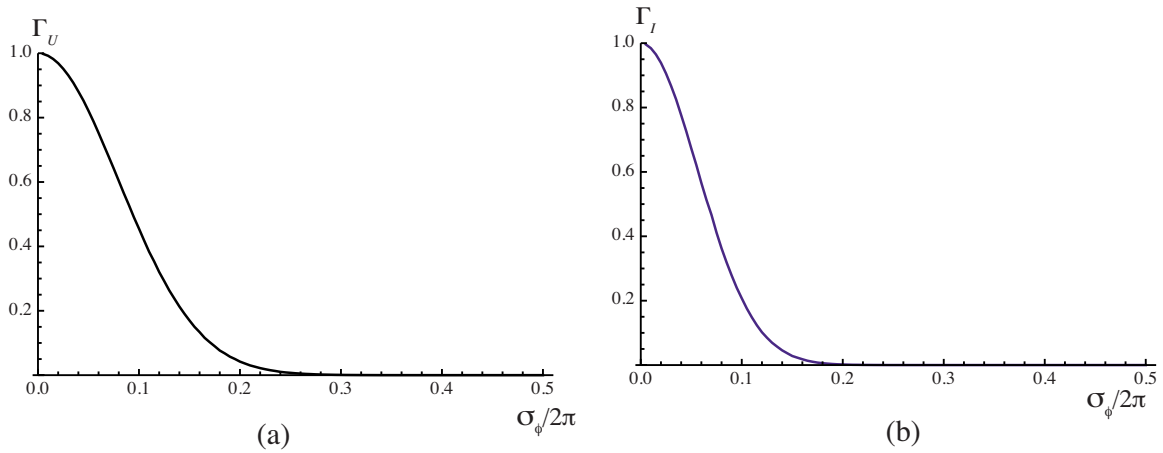

Fig. 3 (a) Magnitude of the correlation of the complex amplitudes of the positive- and negative-frequency components of the spectrum, shown as a function of the normalized standard deviation $\sigma_\phi/2\pi$ of the phase excursions introduced by the diffuser. (b) Similar correlation of the intensities of the Fourier components. These curves are each the result of 100 trials using independent phase sequences of length 2^{20}.

components to the left and right of the specular component. Figure 3(a) shows the magnitude of the correlation Γ_U of positive- and negative-frequency *complex amplitudes* (averaged pair by pair over the spectrum) as a function of the standard deviation of the phase. Figure 3(b) shows the correlation Γ_I of positive- and negative-frequency *intensities*, similarly averaged. Note that correlation of the amplitudes begins to be significant when $\sigma_\phi/2\pi<0.2$, and becomes very high when $\sigma_\phi/2\pi<0.05$.

To summarize this section, when σ_ϕ is large, the specular component becomes very small and there is no symmetry whatsoever to the Fourier intensity $|\tilde{\Phi}(\nu)|^2$, but when σ_ϕ becomes very small, the specular component contains most of the power and the diffuse component of the Fourier intensity approaches even symmetry. This fact is of some interest by itself, but of more interest here is its effect on image-plane speckle for small σ_ϕ.

In the sections that follow, we consider bright-field imaging, dark-field imaging, and imaging with a pupil that is offset from the optical axis. By bright-field imaging we mean imaging with a system that passes the specular component in the Fourier plane and also a portion of the diffuse component, limited by the finite extent of the pupil stop, assumed to be symmetric about the optical axis. By dark-field imaging, we mean imaging with a system that blocks the specular component, but passes a portion of the diffuse component of light, limited again by a finite pupil stop that is symmetrical about the optical axis. Finally, we consider the character of the image speckle when the pupil stop is offset from the optical axis. Again, our goal is to find the effects of Fourier-plane symmetries on the nature of the speckle in the image plane. In particular, our focus is on the *contrast* of the image speckle, which is defined by

$$C=\left(\frac{\overline{I_i^2}-\overline{I_i}^2}{\overline{I_i}^2}\right)^{1/2}, \tag{3}$$

where I_i is the image intensity.

3 Speckle Contrast in Bright-Field Imaging

We first consider the behavior of speckle contrast in bright-field imaging. Of interest is the behavior of speckle intensity contrast as a function of phase standard deviation σ_ϕ for various sizes of pupil stop. Figure 4 shows such curves for a simulation using 2^{20} samples. The quantity F that labels these curves corresponds to the fraction of the total available pupil that is open. More specifically, if the simulation uses length-N sequences, then there are N samples of the spectrum available in the frequency plane. If the pupil allows only P of these samples through to the image plane, then

$$F=P/N. \tag{4}$$

When $F=1$, the pupil stop is wide open; when $F=0$, the pupil is totally closed. Curves with asymptotes below unity correspond to pupils that are a large fraction of the available aperture (F close to unity), while curves with an asymptote near unity correspond to pupils with smaller frac-

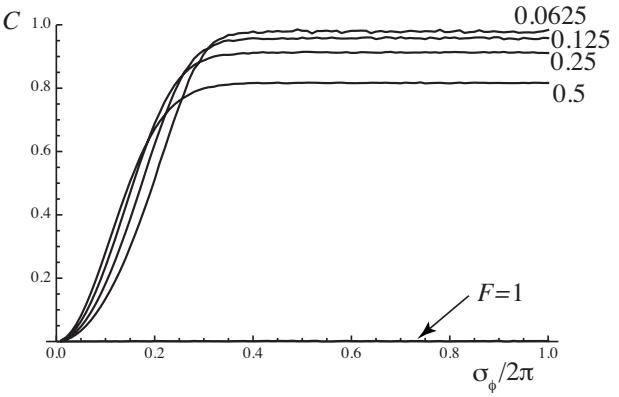

Fig. 4 Speckle intensity contrast versus normalized phase standard deviation in bright-field imaging for various values of the pupil aperture fraction F.

tions of the available aperture open (smaller values of F).

The behavior of these curves contains nothing surprising, and there is no apparent effect of the pupil-plane intensity symmetries for small $\sigma_\phi/2\pi$. The curves all approach zero as σ_ϕ approaches zero, a consequence of the fact that the intensity in this regime is dominated by the very strong specular component transmitted by the pupil. The intensity in the image plane approaches the constant intensity of the specular component, and as a consequence the speckle contrast approaches zero.

The asymptotic behavior when $\sigma_\phi/2\pi$ grows large is also easy to explain. In this case the specular component no longer dominates the image intensity. When F equals unity, the imaging system completely resolves the phase object, and there are no fluctuations of intensity at all for any value of $\sigma_\phi/2\pi$. For values of F that are near unity, the phase structure of the object is partially resolved, and the contrast of the speckle for large phase fluctuations approaches an asymptote that is less than unity, implying that the field statistics are not circular complex Gaussian. When F is a small fraction of unity, the phase fluctuations are totally unresolved, and the speckle contrast for large phase fluctuations approaches that of fully developed speckle. An equivalent viewpoint for large phase fluctuations is that for large F, the point spread function in the object plane is very compact and covers only a small number of scatterers, yielding a contrast that is less than unity, while for small F, the extent of the point spread function is wide in the object plane, embracing many scatterers, and yielding fully developed speckle.

To summarize, there are no apparent effects of Fourier-plane symmetry for small phase fluctuations when bright-field imaging is used. The strong specular component masks any such effects.

4 Speckle Contrast in Dark-Field Imaging

For dark-field imaging, we block the specular component and consider the behavior of the speckle contrast as $\sigma_\phi/2\pi$ is decreased, for various aperture sizes in the pupil plane. Again the aperture size is characterized by the fractional pupil size F.

To begin, we show two speckle intensity patterns obtained by simulation (with length-256 sequences), one for $\sigma_\phi/2\pi=1.0$ and one for $\sigma_\phi/2\pi=0.001$, in Fig. 5. In both cases the fractional pupil opening is $F=0.1$. The characters of the two intensity patterns appear different. One might attribute this to a statistical fluke, but repeated trials with different realizations of phase functions always yield similar differences. When $\sigma_\phi/2\pi=1.0$, the speckle pattern looks quite typical of fully developed speckle. However, when $\sigma_\phi/2\pi=0.001$, the large values seem to exceed the mean value by a greater amount than in part (a), implying a larger speckle contrast.

This observation is confirmed if we calculate the speckle contrast C as a function of $\sigma_\phi/2\pi$ for various values of the fractional pupil opening F, again by simulation with 2^{20} samples, as shown in Fig. 6. Note that as $\sigma_\phi/2\pi\rightarrow 0$, the speckle contrast rises to a value that appears to be $\sqrt{2}$, a phenomenon that must be a consequence of the same factors that led to the Fourier symmetry discussed earlier, or equivalently, a consequence of the real character of the object phase fluctuations.

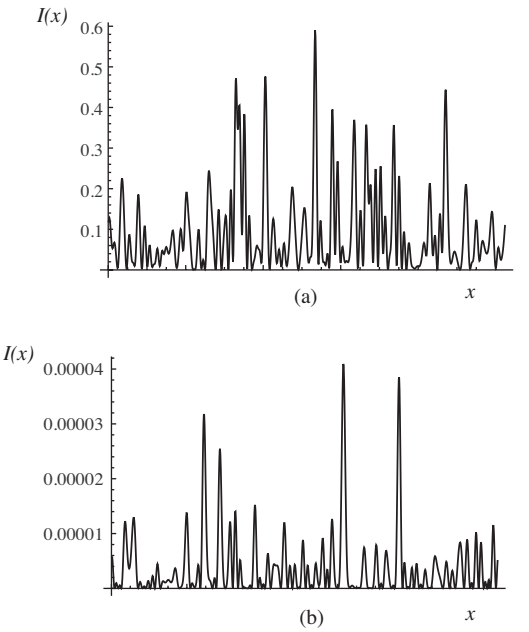

Fig. 5 Speckle intensity patterns when (a) $\sigma_\phi/2\pi=1.0$ and (b) $\sigma_\phi/2\pi=0.001$.

We can derive the limiting value of speckle contrast for very small phase fluctuations using continuous reasoning. For small fluctuations and dark-field imaging, the specular component is suppressed and

$$U_i(x) \approx j\phi(x) \otimes h(x) \equiv j\tilde{\phi}(x), \tag{5}$$

where $U_i(x)$ represents the amplitude of the field in the image plane, $h(x)$ is the amplitude point spread function of the imaging system, and $\otimes$ signifies a convolution operation. For the system shown in Fig. 1, with a symmetrical pupil centered on the optical axis, $h(x)$ is real-valued. It follows that, if $\phi(x)$ is a real-valued Gaussian random process, so too is its linearly filtered version $\tilde{\phi}(x)$. The inten-

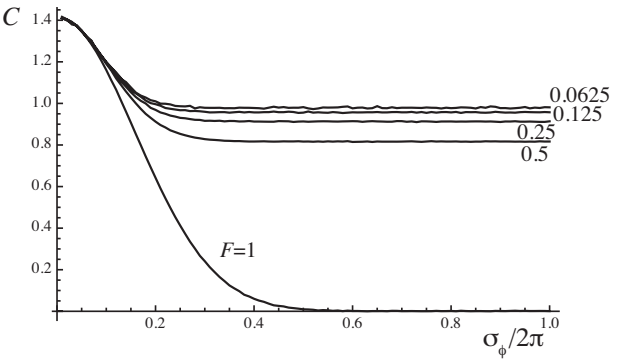

Fig. 6 Speckle intensity contrast as a function of normalized phase standard deviation in dark-field imaging, for various values of the fractional pupil width F. The number of samples used in this simulation was 2^{20}.

sity of the light in the image plane is given by

$$I_i(x) \approx \tilde{\phi}^2(x), \tag{6}$$

and it follows that the mean image intensity is

$$\overline{I_i} = \overline{\tilde{\phi}^2(x)} = \sigma_{\tilde{\phi}}^2, \tag{7}$$

where $\sigma_{\tilde{\phi}}$ is the standard deviation of $\tilde{\phi}(x)$, a result that holds regardless of the probability distribution obeyed by $\tilde{\phi}(x)$. In addition,

$$\overline{I_i^2} = \overline{\tilde{\phi}^4(x)} = 3\sigma_{\tilde{\phi}}^4, \tag{8}$$

where the last step holds only when $\tilde{\phi}(x)$ obeys Gaussian statistics. The contrast in this limiting case can now be calculated as

$$C = \left(\frac{\overline{I_i^2} - \overline{I_i}^2}{\overline{I_i}^2} \right)^{1/2} = \left(\frac{3\sigma_{\tilde{\phi}}^4 - \sigma_{\tilde{\phi}}^4}{\sigma_{\tilde{\phi}}^4} \right)^{1/2} = \sqrt{2}, \tag{9}$$

as suspected from the simulation. Note that even if the statistics of the phase $\phi(x)$ are non-Gaussian, if $h(x)$ is fairly broad in the object plane (i.e., F is small), the statistics of $\tilde{\phi}(x)$ will be close to Gaussian. When F is large and the statistics of $\phi(x)$ are non-Gaussian, the value of C approached at the origin can be different than $\sqrt{2}$.

The fact that the speckle contrast increases as the normalized phase standard deviation approaches zero should not be interpreted as meaning that speckle necessarily becomes a greater impediment to image quality under this circumstance. The total optical power associated with speckle decreases as the phase standard deviation decreases, with more and more of the optical power going into the specular component. The importance of the speckle in image interpretation depends on the strength of the object as well as the standard deviation of the phase.

In summary, we have shown by simulation and continuous reasoning that the contrast of speckle intensity changes as σ_ϕ approaches zero, and that the particular value it approaches is $\sqrt{2}$ in the case of Gaussian phase statistics.

5 Speckle Contrast for Single-Sideband Imaging

A final case we examine by simulation is that of single-sideband imaging, for which only a portion of a single sideband in the frequency domain is passed by the pupil stop. We also assume that the specular component is not transmitted. Such a case can be realized by using a knife-edge in the pupil plane that blocks one half of the pupil (including the specular component), and a slit to control the fraction of the remaining sideband that is transmitted to the image. The open portion of the pupil is now centered on the middle of a single side of the spectrum.

Clearly, in this case symmetry properties of the Fourier spectrum cannot come into play, for only a portion of one side of the spectrum is passed by the system. However, there are some important points to be made by this example, as we shall see.

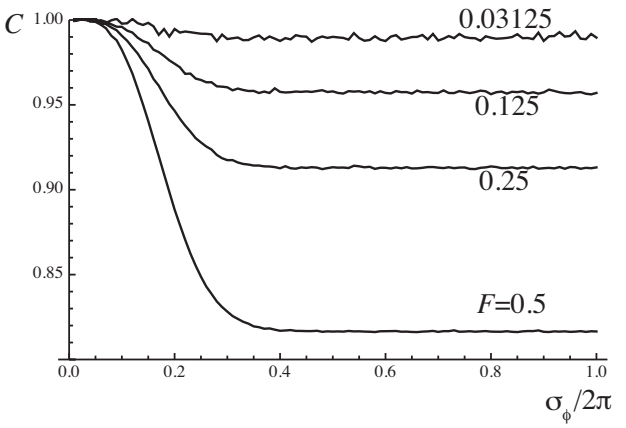

Fig. 7 Speckle intensity contrast versus normalized phase standard deviation for single-sideband imaging and various values of the fractional pupil area F. The number of samples used in this simulation was 2^{23}. Note that the vertical scale extends only from 0.8 to 1.1.

Figure 7 shows the results of a simulation that calculated contrast as a function of $\sigma_\phi/2\pi$ for various values of fractional pupil width F. Note that in this off-axis case the maximum possible value of F is 0.5, and in all cases the specular component was not passed by the system. The phase itself is again assumed to obey zero-mean Gaussian statistics with standard deviation σ_ϕ.

There are two comments to be made about this result. First, as expected, there is no longer a rise above unity in contrast as the phase standard deviation approaches zero, because the spectrum passed by the system has no symmetrical properties. The second comment, which is a bit surprising at first glance, is that the contrast for all curves approaches unity at the origin, which is the contrast expected for fully developed speckle, yet the phase standard deviation becomes vanishingly small in this limit. Why does the speckle remain fully developed even though the object wavefront becomes arbitrarily smooth?

The answer to this question requires a bit of analysis. As in the previous cases, we depend on continuous analysis to explain the result, so as to eliminate aliasing as a possible cause. Figure 8(a) contains the starting point for the analysis, representing a transfer function for the system with the off-axis pupil. The width of the pupil plane is assumed to be $2\nu_0$ (this corresponds to the total number of samples used in the simulation), and within that region, a finite pupil, centered on $\nu_0/2$ with width B, is assumed to exist (this corresponds to the number of pixels P that are transmitted through the pupil). From the definition of the parameter F we see that

$$F = \frac{B}{2\nu_0}. \tag{10}$$

For a given point in the image plane, the weighting function applied in the object plane is the inverse Fourier transform of this transfer function. Since the system is space-invariant and the diffuser is assumed to have stationary statistics, it suffices to consider the image point on axis, in which case the weighting function is

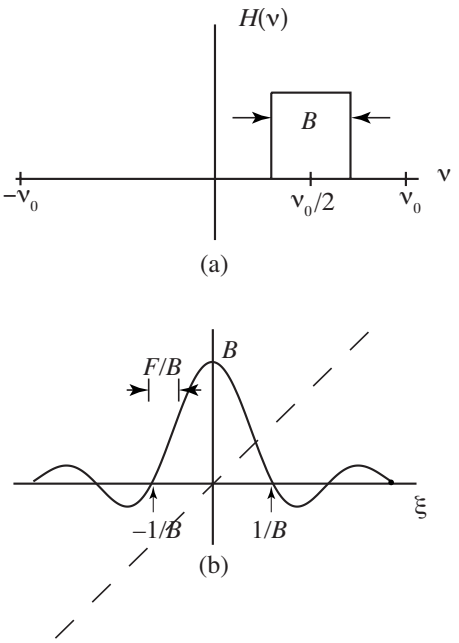

Fig. 8 Explanation of single-sideband results: (a) transfer function for the system with an off-axis pupil; (b) weighting function for the integrand of Eq. (14)—the solid line represents the sinc function, and the dashed line the phase function.

$$h(x) = B\,\mathrm{sinc}Bx\,\exp(-j\pi\nu_0 x), \tag{11}$$

where $\mathrm{sinc}x = (\sin\pi x)/\pi x$. The field amplitude in the image plane is the convolution of this impulse response with the object field

$$U_i(x) = h(x) \otimes U_0(x), \tag{12}$$

where $\otimes$ is a symbol representing the convolution operation. For small phase standard deviation,

$$U_0(x) \approx j\phi(x), \tag{13}$$

assuming that the specular component is not passed by the pupil. The image amplitude on the optical axis can be written

$$U_i(0) \approx j\int_{-\infty}^{\infty} \phi(\xi)B\,\mathrm{sinc}B\xi\,\exp\left(-j\pi\frac{B}{2F}\xi\right)\mathrm{d}\xi, \tag{14}$$

where we have used Eq. (10) in the argument of the exponential.

Figure 8(b) shows the weighting function applied to $\phi(\xi)$ in the integrand for this integration. The solid line represents the sinc function weighting, and the dashed line the phase associated with the exponential function. Note that the sinc function itself also adds π phase shifts in its negative lobes.

Given that the contrast of the speckle is found in the simulations to approach unity as $\sigma_\phi/2\pi$ approaches 0, we expect the speckle fields to approach circular Gaussian complex random variables at any given image point. To prove this, attention should be focused on the real and imaginary parts of $U_i(0)$,

$$\Re_i(0) \approx \int_{-\infty}^{\infty} \phi(\xi)B\,\mathrm{sinc}B\xi\,\sin(\pi B\xi/2F)\mathrm{d}\xi,$$

$$\Im_i(0) \approx \int_{-\infty}^{\infty} \phi(\xi)B\,\mathrm{sinc}B\xi\,\cos(\pi B\xi/2F)\mathrm{d}\xi. \tag{15}$$

Since both $\Re_i(0)$ and $\Im_i(0)$ are integrals of a Gaussian random process, it is clear that they must both obey Gaussian statistics [note that this conclusion can no longer be drawn when the phase fluctuations are too large for the approximation of Eq. (14) to be valid]. But the question remains whether those statistics are circular. For this to be true, the following conditions must hold:

$$\overline{\Re_i(0)} = \overline{\Im_i(0)} = 0,$$

$$\overline{\Re_i^2(0)} = \overline{\Im_i^2(0)},$$

$$\overline{\Re_i(0)\Im_i(0)} = 0. \tag{16}$$

Since the mean of $\phi(\xi)$ is zero by definition, it is clear that $\Re_i(0)$ and $\Im_i(0)$ must have zero means. In Appendix A a proof is given that the second moments of $\Re_i(0)$ and $\Im_i(0)$ are equal and that they are uncorrelated, thus proving the circularity of the statistics.

Hence, when $\sigma_\phi/2\pi \to 0$, the field in the image plane obeys circular complex Gaussian statistics and the contrast is unity, characteristic of fully developed speckle, even though the wavefront deformations are vanishing in this limit.

6 Modeling a Diffuser with Correlated Phases

In the previous section, the diffuser was modeled by a sequence of uncorrelated Gaussian random phases ϕ_k, $k = 1, \ldots, N$, which are then subjected to an exponential transformation to produce $\exp(j\phi_k)$. In the remainder of the paper, we add an additional element to the model, namely a smoothing function that introduces some correlation between phase samples and also reduces the bandwidth of the diffuser spectrum when the phase standard deviation σ_ϕ is small. The particular method of smoothing we have chosen is circular convolution of the length-N uncorrelated phase sequence with a rectangle function of width M. Note that the resulting smoothed phase samples have Gaussian statistics, since convolution of a Gaussian random process with a smoothing function also yields Gaussian statistics. In fact, even if the original uncorrelated phase sequence is non-Gaussian, after convolution with a long enough smoothing sequence, the statistics of the resulting smoothed phase sequence will approach Gaussian, by virtue of the central limit theorem. When particular simulation results are presented, we specify the values of N and M used in the simulation.

When the phase sequence is smoothed, there is an extra phenomenon that changes the detailed character of the curves of contrast C versus $\sigma_\phi/2\pi$, as compared with the results already presented. For large $\sigma_\phi/2\pi$, the correlation interval of the wavefront in the object plane is much smaller than the correlation interval of the phase sequence.

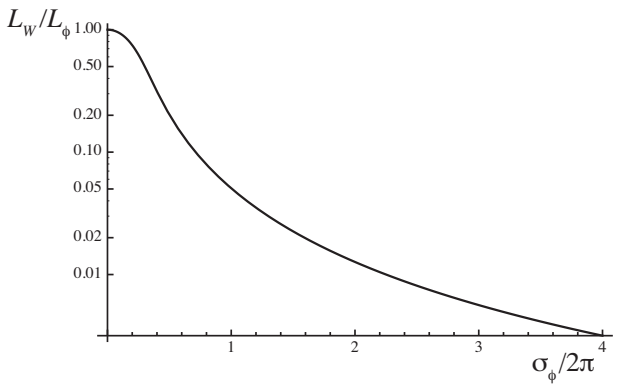

Fig. 9 Correlation length L_W of the wave sequence normalized by the phase correlation interval L_ϕ, as a function of $\sigma_\phi/2\pi$.

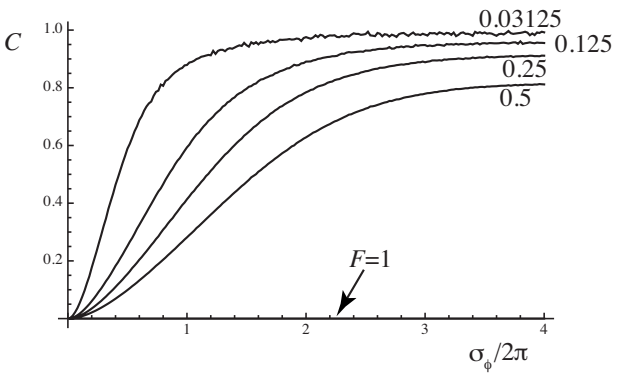

Fig. 10 Speckle intensity contrast C versus $\sigma_\phi/2\pi$ for bright-field imaging and for various fractional pupil widths F. The phase smoothing extends over M=128 pixels, and the total number of pixels in the simulation is $N=2^{20}$.

As shown in the Appendix B, for a rectangular smoothing function of width L applied to the phase sequence, and with Gaussian phase statistics, the ratio of the wave correlation interval L_W to the phase correlation interval L_ϕ is given by

$$\frac{L_W}{L_\phi}=\frac{2[1/\sigma_\phi^2-(1+1/\sigma_\phi^2)\exp(-\sigma_\phi^2)]}{1-\exp(-\sigma_\phi^2)}, \tag{17}$$

which is plotted in Fig. 9. For a rectangular phase smoothing function of length L, the phase correlation length L_ϕ is also equal to L. Note from the figure that when $\sigma_\phi/2\pi \approx 0.7$, the correlation length of the object wave is 1/10 the correlation length of the phase, and when $\sigma_\phi/2\pi \approx 2.2$, the ratio is 1/100. Note also that for small values of $\sigma_\phi/2\pi$, pupil openings smaller than the full pupil width available ($F<1$) can still resolve the smoothed phase variations, with the result that the speckle contrast will remain smaller than unity for a longer interval on the $\sigma_\phi/2\pi$ axis and for smaller values of F than was the case with the uncorrelated phase sequence.

7 Contrast Curves for Smoothed Phase Sequences

In this section we present curves corresponding to Figs. 4, 6, and 7, but for phase sequences that have been smoothed. In all cases, the smoothing is implemented with a rectangular smoothing function of length 128 pixels. This length is sufficient to assure that aliasing plays a negligible role in the results when $\sigma_\phi/2\pi$ is very small.

Figure 10 (to be compared with Fig. 4) shows the bright-field case, plotting contrast C versus $\sigma_\phi/2\pi$ for various values of the fractional pupil opening F. The curve $F=1$ again shows that the speckle contrast vanishes when the pupil is fully open and the correlation function of the wave sequence is fully resolved for all $\sigma_\phi/2\pi$. The curves for smaller values of F increase more slowly with $\sigma_\phi/2\pi$ than do the curves in Fig. 4, but they do approach the same asymptotes in both figures. The reason for the slower rise of contrast with increasing $\sigma_\phi/2\pi$ is that the wavefront deformations resulting from the smoothed phase function are partially resolved for pupils that are smaller than the full pupil opening corresponding to $F=1$, at least for values of $\sigma_\phi/2\pi$ that are small or in an intermediate range.

Figure 11 shows the results for dark-field imaging, which should be compared with Fig. 6. The contrast curves for all values of F again approach $\sqrt{2}$ at the origin, as they do in Fig. 6. The curves also approach the same asymptotes as $\sigma_\phi/2\pi$ grows large. The difference in the smoothed case is primarily the dips observed in the curves in the approximate range $0.2 \leqslant \sigma_\phi/2\pi \leqslant 2$. The dips are again caused by the fact that the correlation length of the wavefront arising from the smoothed phase sequence is partially resolved when F is smaller than unity, until $\sigma_\phi/2\pi$ reaches a large enough value that the correlation length is too small to resolve.

Figure 12 shows the contrast curves for off-axis imaging and a smoothed phase sequence, to be compared with Fig. 7. Again the specular component has been blocked. As $\sigma_\phi/2\pi \to 0$, the contrast curves again all approach unity. Similarly, as $\sigma_\phi/2\pi$ grows large, the curves approach the same asymptotes that were approached in Fig. 7. Again the approach to the asymptotes takes place more slowly than when the phase is not smoothed. Note, however, that the curves for F=0.5, 0.25, and 0.125 have unusual behavior for $\sigma_\phi/2\pi$ in the range $0<\sigma_\phi/2\pi<2$. This behavior is most likely connected with the interaction of the smoothing interval, the shrinking of the wave correlation length as σ_ϕ

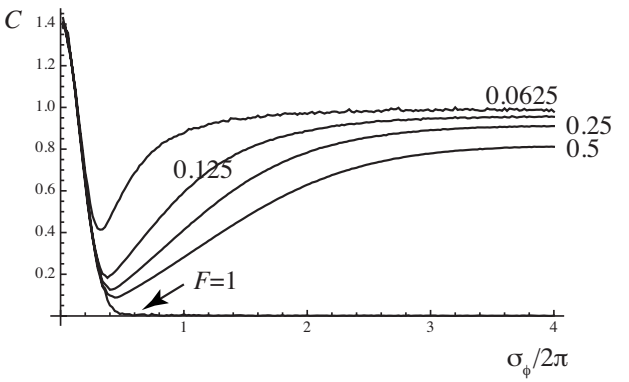

Fig. 11 Speckle intensity contrast C versus $\sigma_\phi/2\pi$ for dark-field imaging and for various fractional pupil widths F. The phase smoothing extends over M=128 pixels, and the total number of pixels in the simulation is $N=2^{20}$.

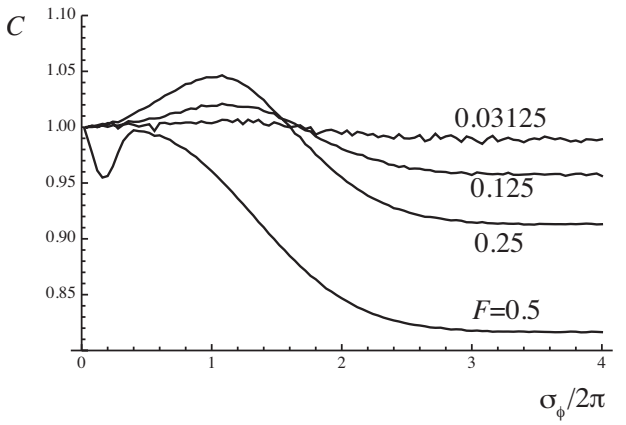

Fig. 12 Curves of contrast C versus normalized phase standard deviation $\sigma_\phi/2\pi$ for various fractional pupil openings F for single-sideband imaging when the specular component is blocked.

increases, and finally the weighting function of the optical system in the object space caused by the finite pupil.

8 Concluding Remarks

We have examined some interesting properties of speckle generated by smooth object wavefronts. If there is a weakness in the arguments presented, it lies in the assumption that we can totally eliminate the specular component of transmitted light in dark-field imaging when the object is extremely smooth. This is easy to do in a simulation, but can be a challenge in a real experiment. Nonetheless, it is of some intrinsic interest to know the properties of speckle when the specular component is removed, and careful experiments can closely approximate this situation in many cases as the fluctuations of $\phi(x)$ become very small.

Appendix A: Proof That the Statistics of the Speckle are Circular in Single-Sideband Imaging with Small Phase Fluctuations

The real and imaginary parts of the field $U_i(0)$ were shown previously to be given by Eq. (15). Our goal here is to find the second moments and cross-correlation of these random variables. As a tool for this task, we first develop a general result that can be applied to both cases. Let a general random variable V be given by

$$V=\int_{-\infty}^{\infty}\phi(\xi)h(\xi)\mathrm{d}\xi, \tag{18}$$

where $h(\xi)$ is a real-valued weighting function and $\phi(\xi)$ is a real-valued, zero-mean, wide-sense stationary random process. It follows that

$$\overline{V^2}=\int\int_{-\infty}^{\infty}\Gamma_\phi(\xi-\eta)h(\xi)h(\eta)\mathrm{d}\xi\,\mathrm{d}\eta, \tag{19}$$

where $\Gamma_\phi(\xi-\eta)=\overline{\phi(\xi)\phi(\eta)}$ is the autocorrelation function of the random process $\phi(\xi)$. With a change of variables

$$\alpha=\xi-\eta,$$

$$\beta=(\xi+\eta)/2, \tag{20}$$

which has a Jacobian of unity, we can perform the integration with respect to β first, yielding

$$\overline{V^2}=\int_{-\infty}^{\infty}\Gamma_\phi(\alpha)\Gamma_h(\alpha)\mathrm{d}\alpha, \tag{21}$$

where $\Gamma_h(\alpha)$ is the deterministic autocorrelation of the known function $h(\xi)$,

$$\Gamma_h(\alpha)=\int_{-\infty}^{\infty}h(\beta+\alpha/2)h(\beta-\alpha/2)\mathrm{d}\beta. \tag{22}$$

To apply this result to the problem at hand, for the real part of $U_i(0)$,

$$h_\Re(\xi)=B\,\mathrm{sinc}B\xi\sin(\pi B\xi/2F), \tag{23}$$

while for the imaginary part,

$$h_\Im(\xi)=B\,\mathrm{sinc}B\xi\cos(\pi B\xi/2F). \tag{24}$$

The simplest way to find the autocorrelation functions of these two functions is to Fourier-transform them, take the magnitude squared of their transforms, and inverse-Fourier-transform the results. For both functions we find the magnitude squared of the transform is

$$|H(\nu)|^2=\frac{1}{4}\mathrm{rect}\left(\frac{\nu-B/4F}{B}\right)+\frac{1}{4}\mathrm{rect}\left(\frac{\nu+B/4F}{B}\right), \tag{25}$$

provided $F\leqslant 1/2$. An inverse transformation of this result yields

$$\overline{\Re^2(0)}=\overline{\Im^2(0)}=\frac{B}{2}\int_{-\infty}^{\infty}\Gamma_\phi(\alpha)\mathrm{sinc}B\alpha\cos\left(\frac{\pi B}{2F}\alpha\right)\mathrm{d}\alpha. \tag{26}$$

To complete a proof of circularity now only requires a demonstration that $\overline{\Re_i(0)\Im_i(0)}=0$, i.e., that the real and imaginary parts of the field are uncorrelated. To accomplish this, we use a generalization of Eq. (21). Consider two random variables defined by

$$V_1=\int_{-\infty}^{\infty}\phi(\xi)h(\xi)\mathrm{d}\xi,$$

$$V_2=\int_{-\infty}^{\infty}\phi(\xi)g(\xi)\mathrm{d}\xi. \tag{27}$$

Then using the same transformation of variables used earlier, we can show that

$$\overline{V_1V_2}=\int_{-\infty}^{\infty}\Gamma_\phi(\alpha)\Gamma_{hg}(\alpha)\mathrm{d}\alpha, \tag{28}$$

where $\Gamma_{hg}(\alpha)$ is the deterministic cross-correlation function of the two weighting functions $h(\xi)$ and $g(\xi)$,

$$\Gamma_{hg}(\alpha) = \int_{-\infty}^{\infty} h(\beta + \alpha/2) g(\beta - \alpha/2) \mathrm{d}\beta. \tag{29}$$

For the case at hand, we have

$$h(\xi) = h_{\Re}(\xi) = B\ \mathrm{sinc} B\xi \sin(\pi B\xi/2F),$$

$$g(\xi) = h_{\Im}(\xi) = B\ \mathrm{sinc} B\xi \cos(\pi B\xi/2F). \tag{30}$$

Again, to evaluate the cross-correlation integral, we move to the frequency domain. The Fourier transforms needed are

$$H(\nu) = \mathrm{rect}(\nu/B) \otimes \left[\frac{1}{2j}\delta(\nu - B/4F) - \frac{1}{2j}\delta(\nu + B/4F) \right]$$
$$= \frac{1}{2j}\left[\mathrm{rect}\left(\frac{\nu - B/4F}{B} \right) - \mathrm{rect}\left(\frac{\nu + B/4F}{B} \right) \right], \tag{31}$$

$$G(\nu) = \mathrm{rect}(\nu/B) \otimes \left(\frac{1}{2}\delta(\nu - B/4F) + \frac{1}{2}\delta(\nu + B/4F) \right)$$
$$= \frac{1}{2}\left[\mathrm{rect}\left(\frac{\nu - B/4F}{B} \right) + \mathrm{rect}\left(\frac{\nu + B/4F}{B} \right) \right]. \tag{32}$$

Provided $F \leqslant 1/2$, there is no overlap between the two rectangle functions that occur in each equation, and as a result

$$H(\nu)G(\nu) = \frac{1}{4j}\left[\mathrm{rect}\left(\frac{\nu - B/4F}{B} \right) - \mathrm{rect}\left(\frac{\nu + B/4F}{B} \right) \right]. \tag{33}$$

An inverse transformation now yields

$$\Gamma_{hg}(\alpha) = B\ \mathrm{sinc} B\alpha \sin(\pi B\alpha/2F). \tag{34}$$

When this equation is substituted into Eq. (28), we find

$$\overline{\Re_i(0)\Im_i(0)} = \int_{-\infty}^{\infty} \Gamma_\phi(\alpha) B\ \mathrm{sinc} B\alpha \sin(\pi B\alpha/2F) \mathrm{d}\alpha = 0, \tag{35}$$

where the final step results from the odd symmetry of the integrand.

Thus we have proved that for small $\sigma_\phi/2\pi$, the field $U_i(0)$ is a circular complex random variable. By stationarity of $\phi(x)$, the same is true at all points of the image.

Appendix B: Wave Correlation Length in Terms of the Phase Correlation Length

From Ref. 10, Eq. (4-106), the normalized wave correlation function can be expressed in terms of the normalized phase correlation function as follows:

$$\mu_W(\Delta x) = \frac{\exp[-\sigma_\phi^2(1 - \mu_\phi(\Delta x)\ ] - \exp(-\sigma_\phi^2)}{1 - \exp(-\sigma_\phi^2)}. \tag{36}$$

For smoothing with a rectangular weighting function of width L, the normalized correlation function of the phase is easily shown to be

$$\mu_\phi(\Delta x) = \begin{cases} 1 - |\Delta x|/L, & |\Delta x| < L, \\ 0 & \text{otherwise}. \end{cases} \tag{37}$$

The correlation length of the phase, L_ϕ, is the area under $\mu_\phi(\Delta x)$, which in this case yields $L_\phi = L$.

The correlation length of the wave, L_W, is the area under $\mu_W(\Delta x)$. Given the symmetry of $\mu_\phi(\Delta x)$, this integral can be written

$$L_W = 2\int_0^{L_\phi} \frac{\exp(-\sigma_\phi^2 \Delta x/L_\phi) - \exp(-\sigma_\phi^2)}{1 - \exp(-\sigma_\phi^2)} \mathrm{d}\Delta x. \tag{38}$$

The integration can be performed and yields

$$\frac{L_W}{L_\phi} = \frac{2[1/\sigma_\phi^2 - (1 + 1/\sigma_\phi^2)\exp(-\sigma_\phi^2)]}{1 - \exp(-\sigma_\phi^2)}, \tag{39}$$

as asserted in Eq. (17).

References

1. H. Fujii, T. Asakura, and Y. Shindo, "Measurement of surface roughness properties by using image speckle contrast," *J. Opt. Soc. Am. A* **66**, 1217–1222 (1976).
2. H. Fujii, J. Uozumi, and T. Asakura "Computer simulation study of image speckle patterns with relation to object surface profile," *J. Opt. Soc. Am. A* **66**, 1222–1236 (1976).
3. H. M. Pederson, "Theory of speckle dependence on surface roughness," *J. Opt. Soc. Am. A* **66**, 1204–1210 (1976).
4. J. W. Goodman, "Dependence of image speckle contrast on surface roughness," *Opt. Commun.* **14**, 324–327 (1975).
5. W. T. Welford, "Laser speckle and surface roughness," *Contemp. Phys.* **21**, 401–412 (1980).
6. A. Boccaletti, P. Riaud, and D. Rouan, "Speckle symmetry with high-contrast coronagraphs," *Publ. Astron. Soc. Pac.* **114**, 132–136 (2002).
7. A. Sivaramakrishnan, P. E. Hodge, R. B. Makidon, M. D. Perrin, J. P. Lloyd, E. E. Bloemhof, and B. R. Oppenheimer, "The adaptive optics point-spread function at moderate and high Strehl ratios," in *High-Contrast Imaging for Exo-Planet Detection*, A. B. Schultz and R. G. Lyon, Eds. *Proc. SPIE* **4680**, 161–170 (2003).
8. E. E. Bloemhof, "Suppression of speckles at high adaptive correction using speckle symmetry," in *Instruments, Methods, and Missions for Astrobiology IX*, R. B. Hoover, G. V. Levin, and A. Y. Rozanov, Eds., *Proc. SPIE* **6309**, 63090X (2006).
9. J. W. Goodman, *Statistical Optics*, John Wiley & Sons, New York (1985).
10. J. W. Goodman, *Speckle Phenomena in Optics*, Roberts & Company, Englewood, CO (2007).

Joseph W. Goodman joined the faculty of the Department of Electrical Engineering at Stanford University in 1967. He chaired the department from 1989 to 1996, and then served as senior associate dean of engineering until 2000. He retired from Stanford in 2001. He is the author of the books *Introduction to Fourier Optics* (now in its third edition), *Statistical Optics*, and *Speckle Phenomena in Optics*, and coauthor of *Fourier Transforms: An Introduction for Engineers*. He has received numerous awards from the IEEE, the ASEE, the OSA, and SPIE, including the highest awards given by the last two societies. He was a cofounder of Optivision, Inc., and ONI Systems, and served as a member of the board of directors of E-TEK Dynamics.